The phase diagram and critical behaviour of the easy-plane antiferromagnet $CsNi_{0.98}Fe_{0.02}Cl_3$

1997 J. Phys.: Condens. Matter 9 703

(http://iopscience.iop.org/0953-8984/9/3/010)

J. Phys.: Condens. Matter **9** (1997) 703–713. Printed in the UK PII: S0953-8984(97)77921-9

The phase diagram and critical behaviour of the easy-plane antiferromagnet $CsNi_{0.98}Fe_{0.02}Cl_3$

M Winkelmann†, R Schneider‡, M Enderle‡, T Asano§, Y Ajiro§ and M Steiner†

† Hahn-Meitner-Institut, Glienicker Strasse 100, D-14109 Berlin, Germany
‡ Technische Physik, Universität des Saarlandes, D-66123 Saarbrücken, Germany
§ Department of Applied Physics, Fukui University, Fukui 910, Japan

Received 18 September 1996

Abstract. Neutron diffraction measurements have been performed to determine the magnetic phase diagram of the stacked-triangular antiferromagnet $CsNi_{0.98}Fe_{0.02}Cl_3$ between $T = 1.8$ K and $T = 6$ K in static magnetic fields up to $B = 5$ T applied perpendicular to the c-axis. The substitution of a few per cent of Fe^{2+} for Ni^{2+} leads to a compensation of the weak Ising anisotropy of the pure compound, and induces an XY-anisotropy in the doped system. The magnetic phase diagram displays three different magnetically ordered phases with a multicritical point at $B = 2$ T and $T = 4.3$ K. The phase diagram and the spin configurations of the different phases are found to be consistent with theoretical predictions for stacked-triangular antiferromagnets with a weak easy-plane anisotropy. The spin ordering at zero field exhibits a 120° structure in the basal plane with inherent XY- and chiral degeneracy. We have determined the critical exponent of the sublattice magnetization to be $\beta = 0.23(1)$, which is close to the theoretical value $\beta = 0.25$ of an XY chiral antiferromagnet.

1. Introduction

In hexagonal ABX_3 compounds the presence of spin frustration resulting from antiferromagnetic coupling in the stacked-triangular lattice causes a rich variety of phase transitions [1] including new universality classes linked to the chiral degeneracy inherent to the 120° ordered spin structure [2]. The magnetic phase transitions in stacked-triangular lattice antiferromagnets (STAL-AF) depend remarkably on the spin symmetry and anisotropy [3, 4]. The compounds $RbMnBr_3$ [5] and $CsMnBr_3$ [6] with XY-anisotropy exhibit a single transition at zero field characterized by novel critical exponents, which splits into two successive transitions under a finite magnetic field applied in the basal plane. In contrast, $CsNiCl_3$ [7], $CsNiBr_3$ and $CsMnI_3$ [8, 9] with Ising anisotropies show two successive transitions at zero fields, merging into a single transition at a multicritical point for a finite field parallel to the c-axis. In addition, a line of spin-flop transitions is linked to this point. Although the strength of the anisotropy is different, scaled phase diagrams display a universal behaviour in each case except for an additional phase boundary associated with an incommensurate spin structure in $RbMnBr_3$ [4]. From this point of view, it is interesting to study the effect of anisotropy on the magnetic phase transitions of a typical ABX_3 substance by systematically varying the anisotropy in a continuous manner. This can be achieved by the substitution for a certain amount of B ions with magnetic ions with a different kind of single-site anisotropy in order to tune the effective anisotropy of the system.

0953-8984/97/030703+11$19.50

The effectiveness of this method is caused by the fact that the compounds are quasi-1d antiferromagnets, where the magnetic moments interact strongly in the stacking direction c, thereby averaging the anisotropy over many ions. It should be noted, however, that random substitution inevitably makes the system more or less inhomogeneous. Recently, an ultrasonic study of the magnetic phase diagrams of $CsNi_{0.98}M_{0.02}Cl_3$ (M = Co, Fe, Mg) has been reported by Trudeau *et al* [10]. Here, the Fe-doped compound is of special interest, because this system changes to XY-anisotropy, while Co- and Mg-doped samples display phase diagrams with the same general features as the Ising-type $CsNiCl_3$. As stated by Trudeau *et al*, the Fe^{2+} ions are known to exhibit a strong XY-anisotropy in the ABX_3 matrix, cf. e.g. $CsFeCl_3$ [11]. Since the Ising-like behaviour of $CsNiCl_3$ is weak, a compensation is easily possible. As a result, the observed phase diagram of $CsNi_{0.98}M_{0.02}Cl_3$ presents characteristics of the STAL-AF with XY-anisotropy such as $CsMnBr_3$ and $RbMnBr_3$.

Here, we report neutron diffraction results on $CsNi_{0.98}Fe_{0.02}Cl_3$ clarifying the magnetic phase diagram and the spin structures of the three different ordered phases. In addition, the critical exponent β of the sublattice magnetization has been determined to confirm the chiral degeneracy of the zero-field structure.

2. Experiment

We used for this experiment the double-axis diffractometer E4 at BENSC. A wavelength $\lambda = 2.46$ Å was selected by a pyrolytic graphite (PG) monochromator. Higher-order wavelength contributions were suppressed by using a PG filter. The beam collimation was chosen to be 40′–40′–40′. Our single-crystal sample with a volume of approximately 0.3 cm^3 was mounted in a vertical cryomagnet with $(1, 1, 0)$ and $(0, 0, 1)$ reciprocal-lattice vectors in the scattering plane. The deviation from an ideal 90° orientation between the field and the c-axis was smaller than 1°. The intensities at the magnetic Bragg positions $(1/3, 1/3, 1)$ and $(4/3, 4/3, 1)$ were measured as a function of temperature ($1.8\ \text{K} \leqslant T \leqslant 6\ \text{K}$) and magnetic field ($0\ \text{T} \leqslant B \leqslant 5\ \text{T}$). In addition, the integrated intensities of several magnetic Bragg reflections were determined at certain points of the (B, T) phase diagram. To obtain the critical exponent β the $(1/3, 1/3, 1)$ reflection was measured at zero field by scanning along $(1, 1, 0)$. The temperature stability was better than $\Delta T = \pm 3$ mK in the range of interest between 4 K and 5.5 K.

3. Results

Figures 1 and 2 show the intensities at the magnetic Bragg positions $(1/3, 1/3, 1)$ and $(4/3, 4/3, 1)$ versus temperature for different magnetic fields applied along $(-1, 1, 0)$. Two phase transitions I–II and II–III are clearly visible up to $B \approx 2$ T in the temperature dependence of both reflections. Above $B = 2$ T a new transition (II–IV) appears slightly below the phase boundary between the ordered and the paramagnetic phase. The spin reordering leads to an increase of the intensity of the $(4/3, 4/3, 1)$ Bragg reflection, while it has almost no effect on the $(1/3, 1/3, 1)$ reflection. Hence a spin component perpendicular to $(4/3, 4/3, 1)$ but not to $(1/3, 1/3, 1)$ must be involved at the II–IV transition. Considering that $(1/3, 1/3, 1)$ contains a large $(0, 0, 1)$ component, while $(4/3, 4/3, 1)$ is mainly along $(1, 1, 0)$, we conclude that the low-temperature structure IV involves an ordered z-component of the spins. The smooth increase of the slope of the sublattice magnetization indicates a broadened transition. Therefore, the transition temperatures T_{N1} and T_{N2} were

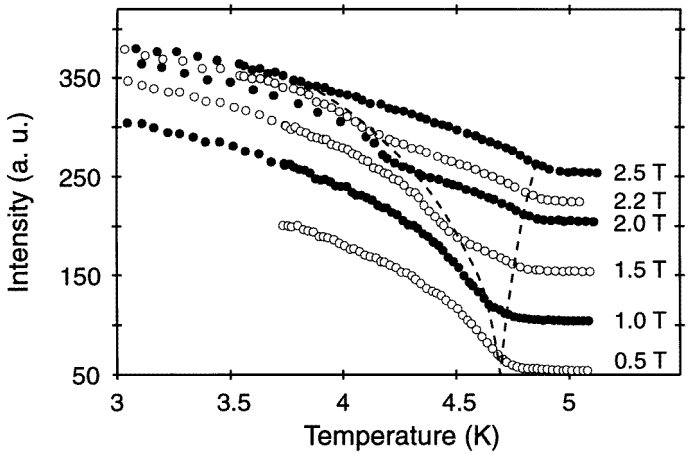

Figure 1. Intensities at the magnetic Bragg position $(1/3, 1/3, 1)$ versus temperature at magnetic fields up to $B = 2.5$ T.

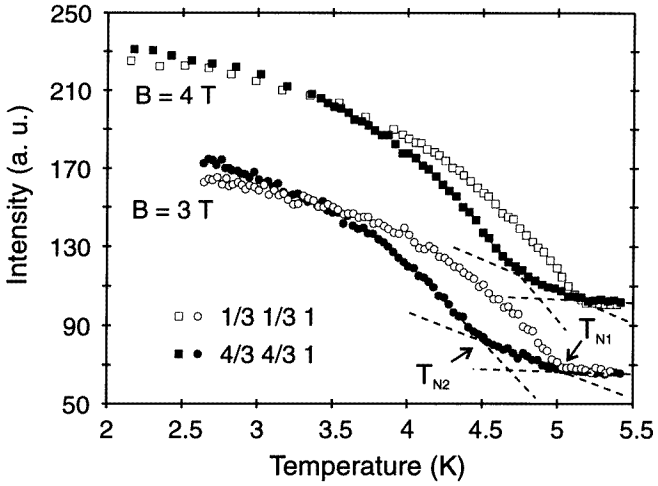

Figure 2. Intensities at the magnetic Bragg positions $(1/3, 1/3, 1)$ and $(4/3, 4/3, 1)$ versus temperature at high magnetic fields. A second phase transition is indicated by the sudden increase of the intensity of the $(4/3, 4/3, 1)$ reflection.

determined by fitting two lines with different slopes and one line for the constant background above T_{N1} to the intensity curves around the phase transitions (see figure 2).

Field scans at constant temperature were performed to determine the phase boundary at low temperatures. The measurements show a broad transition, as is visible in figure 3. The intensity decreases gradually from a higher plateau in phase III to a lower one in phase IV. This behaviour could either indicate a smeared transition, or two transitions with an intermediate phase. To illustrate both possibilities, we determined the transition region with one critical field B_c at the point of inflection and two threshold fields B_{t1} and B_{t2} at 5% and 95% of the total intensity decrease. The resulting phase diagram is presented in figure 4.

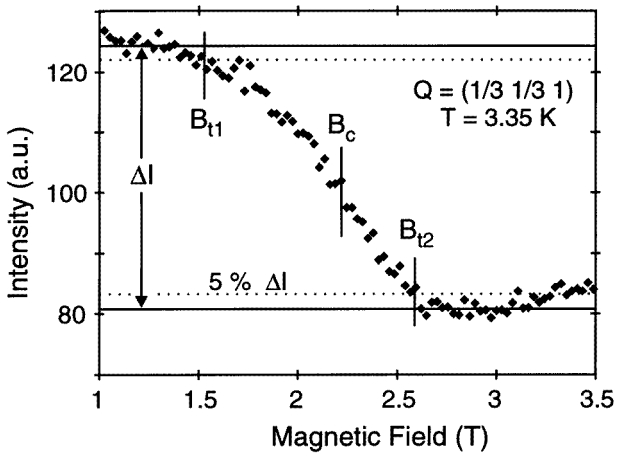

Figure 3. The intensity at the magnetic Bragg position $(1/3, 1/3, 1)$ versus the magnetic field.

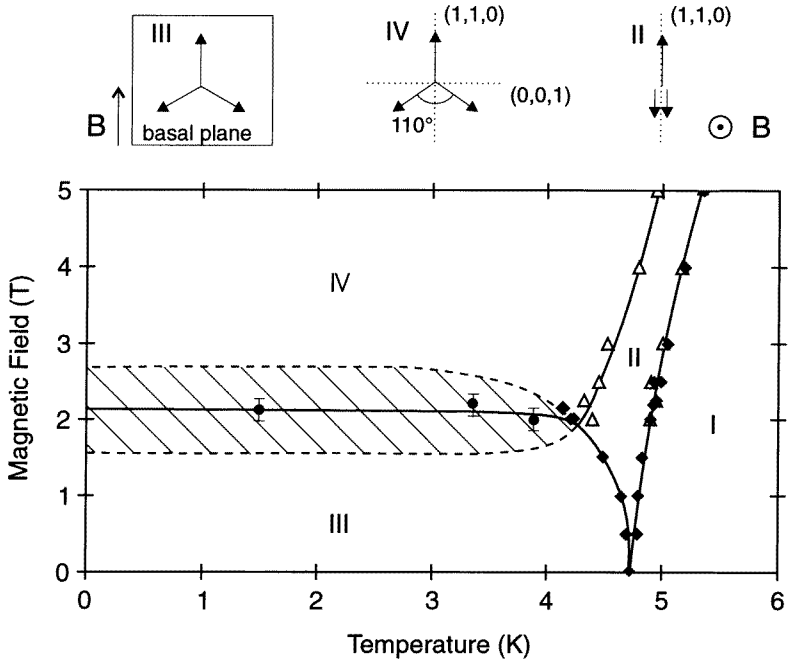

Figure 4. The magnetic phase diagram of $CsNi_{0.98}Fe_{0.02}Cl_3$. The shaded area represents the width between 5% and 95% of the whole intensity decrease of the phase transition.

Three phase boundaries meet at the multicritical point $B = 2.0(2)$ T and $T = 4.3(1)$ K.

The observed Bragg intensities measured at different points of the (B, T) diagram are listed in table 1. We found the data at zero field to be in good agreement with the calculated intensities of the expected helical structure in the basal plane (R = 4.9%). For all calculations the isotropic approximation of the ionic Ni^{2+} form factor was used [12]. The

Table 1. The magnetic intensities observed at different points of the phase diagram compared to the calculated intensities for the models shown in figure 4: $B = 0$ T, $T = 1.8$ K (phase III), $B = 3.5$ T, $T = 1.8$ K (phase IV), $B = 3.5$ T, $T = 4.80$ K (phase II). The R-factor is defined as $R = \sum(I(\text{obs}) - I(\text{calc}))^2 / \sum I(\text{obs})^2$. I'(calc) for phase II is explained in the text.

Phase:	III		IV		II		
hkl	I(obs)	I(calc)	I(obs)	I(calc)	I(obs)	I(calc)	I'(calc)
1/3 1/3 1	967	986	591	604	189	201	192
2/3 2/3 1	577	570	398	398	86	83	88
4/3 4/3 1	204	210	171	172	18	14	21
7/3 7/3 1	—	68	88	60	8	2	5
1/3 1/3 3	272	221	159	126	61	51	47
2/3 2/3 3	204	191	122	112	42	42	39
4/3 4/3 3	136	121	92	77	—	—	—
R-factor		4.9%		6.2%		7.2%	6.9%

intensities measured at $B = 3.5$ T and $T = 1.8$ K favour a slightly distorted helical structure perpendicular to the field axis. In this structure one of the three spins on a triangle points along $(1, 1, 0)$ and the other two enclose an angle of $\pm 55(2)^\circ$ with $(-1, -1, 0)$, as shown in the upper part of figure 4. The R-factor obtained is 6.2%, whereas $R = 7.2\%$ is calculated for a 120° structure perpendicular to the field direction. The finite easy-plane anisotropy causes this slight deviation from the 120° order. An additional canting towards the field axis can be expected, giving rise to scattering contributions at nuclear Bragg positions. However, the strong nuclear intensity masks this small magnetic contribution, which could not be detected even at $B = 5$ T. The spin ordering in phase II will be discussed in the next section in comparison with theoretical predictions.

The temperature dependence of the zero-field order parameter was studied by scanning the $(1/3, 1/3, 1)$ reflection along $(h, h, 0)$ (perpendicular to the chain axis c) at different temperatures. Figure 5 shows the data at $T = 4.70$ K very close to T_N after subtraction of a constant background. Integrated intensities were obtained by fitting the data using a Gaussian with fixed width for the Bragg intensity and a Lorentzian for the critical scattering. The width of the Gaussian and the constant background were determined at the base temperature of the ^{4}He cryostat, $T = 1.8$ K. Although the correction of the critical scattering is essential only very close to T_N, all scans were treated using the same two-profile fit. The chosen counting times were optimized for good statistics of the Bragg intensities, and were not sufficient for an accurate determination of the temperature dependence of the critical scattering. No significant effect due to extinction, which can be a source of serious error in the determination of β, was observed after the refinement of the magnetic zero-field structure, where an empirical extinction factor was used as an additional parameter. The Gaussian integrated intensity is shown in figure 6 versus reduced temperature. A least-squares fit with the power law $I \propto ((T - T_N)/T_N)^{2\beta}$ gives $T_N = 4.66(2)$ K and $\beta = 0.23(1)$. However, deviations from a straight line are visible in the double-logarithmic plot. Moreover, some Bragg intensity remains above the value determined for T_N. Obviously, the random distribution of Fe^{2+} ions on Ni sites causes a broadening of the Néel temperature. This is reasonable because the random distribution of the Fe^{2+} ions on the Ni sites could lead to local variations in the effective interactions and anisotropy. We have tried to convolute the power law with a Gaussian distribution

of T_N. The fit shows an excellent agreement with the data for a Gaussian broadening of $(\mathrm{FWHM})_{T_N} = 2.35\sigma = 0.172(2)$ K (figure 6(b)), and gives the same values, $\beta = 0.23(1)$ and $T_N = 4.67(2)$ K, as determined above. Note that $(\mathrm{FWHM})_{T_N}$ is still much smaller than the difference of the two Néel temperatures of the pure compound, $T_{N1} = 4.84$ K and $T_{N2} = 4.40$ K. This confirms that the phase boundaries I–II and II–III do indeed merge into a single phase transition at zero field.

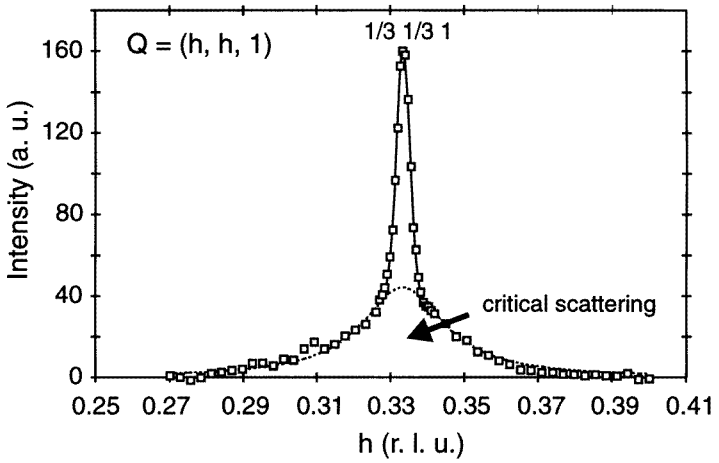

Figure 5. The $(1/3, 1/3, 1)$ magnetic Bragg reflection with critical scattering measured at $T = 4.70$ K. The data are fitted by a Gaussian plus a Lorentzian. The width of the Gaussian is fixed to the value at the base temperature ($T = 1.8$ K).

Close to $B = 0$, the phase boundaries I–II and II–III follow a power law $H^2 = A_i|T - T_N|^{\phi_i}$ where i = I–II, II–III, respectively. We obtain $\phi_{I-II} = 1.12(10)$ and $\phi_{II-III} = 1.01(30)$ using data for below 2 T. For this analysis, the Néel temperature at $B = 0$ was determined using the same method as for the field data, giving a somewhat higher value of $T_N = 4.75$ K compared to T_N determined above.

4. Discussion

The phase boundaries I–II, II–III and III–IV are in good agreement with the phase diagram determined recently from ultrasonic experiments [10]. The phase boundary II–IV, however, was not detectable in the ultrasonic velocity data. In the low-field part, the phase diagram resembles those of other hexagonal XY-antiferromagnets, $CsMnBr_3$, $RbMnBr_3$ and $CsVX_3$, which all show the tetracritical point at $B = 0$ and have the 120° helical structure and a distorted helical structure at zero and low-field values, respectively. The phase transition II–IV does not appear in these systems, indicating a significant difference between $CsNi_{0.98}Fe_{0.02}Cl_3$ and all other known STAL-AF with easy-plane anisotropy. Note that the phase diagram of $RbMnBr_3$ is further complicated by an incommensurate–commensurate phase transition, which is caused by deviations from the hexagonal symmetry in the (a, b) plane. Hence the phase diagram is only accidentally similar to that of $CsNi_{0.98}Fe_{0.02}Cl_3$.

An overview of the variety of possible phase diagrams for triangular lattices obtained as the anisotropy is varied has been given by Plumer *et al* on the basis of a Landau-type mean-field theory [1]. A phase diagram with three ordered phases, similar to the observed

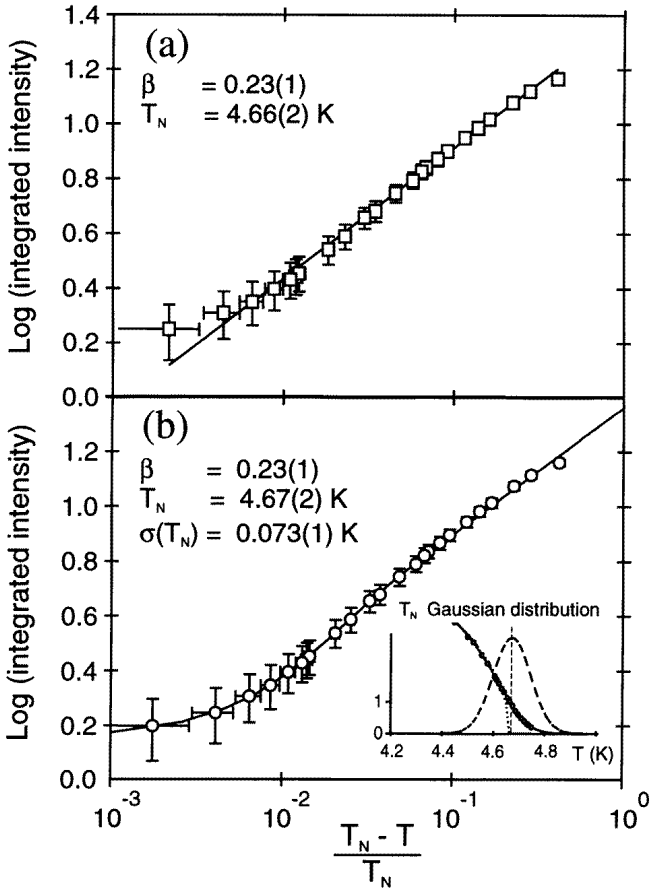

Figure 6. A double-logarithmic plot of the (1/3, 1/3, 1) magnetic Bragg intensity versus reduced temperature. Two different fits were used to determine the critical exponent β and T_N: a pure power law $I \propto ((T_N - T)/T_N)^{2\beta}$ (a), and a power law convoluted with a Gaussian distribution of T_N due to the random substitution of Fe^{2+} for Ni^{2+} (b).

one, is included in this theory for the case of a weak XY-anisotropy, whereas only two ordered phases appear in case of a strong anisotropy. The phases II, III, IV correspond to the notation 5, 7 and 3, respectively. Additional anisotropy terms up to fourth order can produce more complex phase diagrams, including the appearance of an intermediate phase 8 between phases 7 and 3 (III and IV).

The detailed reorientation processes of hexagonal antiferromagnets with weak XY-anisotropy due to an applied magnetic field have been studied in recent papers using a Landau theory on the basis of the Heisenberg Hamiltonian

$$H = 2J \sum_i S_i S_{i+1} + 2J' \sum_{i \neq j} S_i S_j + D \sum_i (S_1^z)^2 - H \sum_i S_i. \tag{1}$$

Rastelli and Tassi [13] numerically determine the $T = 0$ minimum of the classical energy, while Abarzhi and Chubukov [14] give their results up to first order in the reduced parameters $d = D/2J$ and $j = J'/J$. Their results are generally the same, but they differ with respect to the explicit values of the transition fields. In agreement with [1], both

[13] and [14] predict two ordered phases in the case of strong XY-anisotropy, a (distorted) helix phase H and a fan phase F, while in the weak-anisotropy case $D < D_0 \approx 3J'$ an additional phase, the umbrella phase U, should appear between the distorted helix and the fan phase. The phase transition between H and U is of first order and all other phase transitions should be second order. For a comparison of our experimental results with the theoretical predictions we used the equations given in [13]. The six spins of the magnetic unit cell can be represented by classical vectors $\boldsymbol{S} = S(\sin\theta_s \sin\phi_s, \sin\theta_s \cos\phi_s, \cos\theta_s)$ with $\boldsymbol{x} \parallel (1, 1, 0)$, $\boldsymbol{y} \parallel (-1, 1, 0) \parallel \boldsymbol{B}$, and $\boldsymbol{z} \parallel (0, 0, 1)$. The minimum of the free energy is related to certain restrictions between the polar and azimuthal angles, which are

$$\begin{aligned} &\theta_s = 90^\circ \qquad s = 1, \ldots, 6 \\ &\phi_4 = -\phi_1 \qquad \phi_5 = -\phi_3 \qquad \phi_6 = -\phi_2 \end{aligned} \tag{2}$$

for the H phase, additionally $\phi_2 = \phi_3$ for the F phase, and

$$\begin{aligned} &\theta_4 = \theta_1 = 90^\circ \qquad \theta_6 = \theta_2 = 180^\circ - \theta_5 = 180^\circ - \theta_3 \\ &\phi_4 = -\phi_1 \qquad \phi_5 = \phi_6 = -\phi_2 = -\phi_3. \end{aligned} \tag{3}$$

for the U phase. Thus, the spin configurations are characterized by only three (two) azimuthal angles in the H (F) phase, and one polar and two azimuthal angles in the U phase. These angles are determined by the parameters B/J, J'/J and D/J.

The spin structure of the H phase at $B = 0$ is the antiferromagnetic 120° structure, which distorts at finite field, but remains in the easy plane. We conclude from our zero-field results on $CsNi_{0.98}Fe_{0.02}Cl_3$ that phase II corresponds to the H phase.

In the umbrella phase U, one spin of a triangle (S_1) is in the basal plane, while the other two (S_2, S_3) include an angle of $90^\circ - \theta_2 < 60^\circ$ with the basal plane. Our refinement of the intensity data measured at $B = 3.5$ T and $T = 1.8$ K (phase IV) is in agreement with this structure for a canting angle $\theta_2 = 35(2)^\circ$. The azimuthal angles ϕ_1 and ϕ_2 correspond predominantly to a spin rotation towards the field axis resulting in a ferromagnetic component, and, thus, could be only roughly estimated ($0^\circ < \phi_1, 180^\circ - \phi_2 < 10^\circ$). We have used equations (2.6) and (2.8) of [13] to estimate D from the polar angle determined, $\theta_2 = 35(2)^\circ$, and the coupling constants, $J'/k_B = 0.29$ K and $J/k_B = 16.6$ K, of pure $CsNiCl_3$ [15]. Since the phase transition temperatures of $CsNiCl_3$ and $CsNi_{0.98}Fe_{0.02}Cl_3$ are almost the same, we do not expect significant differences between their exchange interactions J' and J.

The calculation yields the values $D/k_B = 0.2(1)$ K, $\phi_1 \approx 2^\circ$, and $\phi_2 \approx 176^\circ$. However, this anisotropy value corresponds to a transition field of about 5 T between the distorted helix and umbrella phase, considerably higher than the observed transition field of about 2.2(5) T. The observed transition field requires $D/k_B = 0.03(2)$ K and leads to a canting angle $\theta_2 = 30.5(5)^\circ$, which is not consistent with our intensity data. A part of this discrepancy might be attributed to the application of $T = 0$ calculations to explain data taken at finite temperatures. A temperature-dependent canting angle is known to exist in hexagonal antiferromagnets with weak Ising anisotropy [16, 17], where the canting angle with respect to the Ising axis increases slightly when one lowers the temperature. A similar effect can be expected in the umbrella phase of the weak XY-antiferromagnet, because the easy-plane anisotropy combined with the magnetic field induces an effective Ising anisotropy along $\boldsymbol{x}$. Thus, the discrepancy might be reduced at lower temperature. On the basis of the present analysis we, therefore, estimated $0.03\ \text{K} < D/k_B < 0.2$ K.

The fan phase F is characterized by a collinear order along $\boldsymbol{x}$ with the propagation vector $(1/3, 1/3, 1)$. In the classical $T = 0$ treatment this phase occurs for weak anisotropies in a narrow field range slightly below the saturation field. Since the fan structure can be

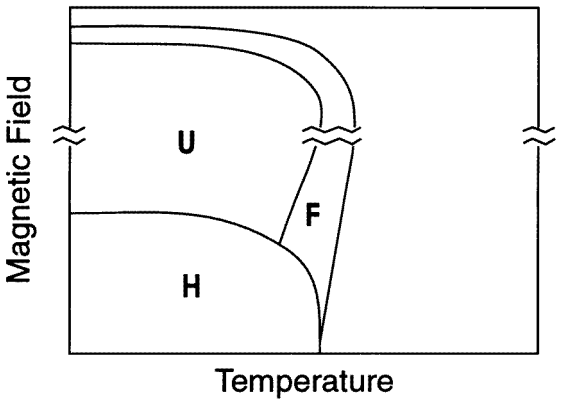

Figure 7. A schematic plot of the expected phase diagram of hexagonal XY-antiferromagnets with weak anisotropy ($D < 3J'$) with the notation of Rastelli and Tassi.

identified with phase 5 in the low-field results of Plumer *et al*, we expect the schematic phase diagram to look like the one illustrated in the figure 7. At low fields and high temperature a spin component perpendicular to $\boldsymbol{x}$ remains disordered. The partial order can be compared to the intermediate phase of $CsNiCl_3$, where only the spin component along the Ising axis is ordered, while the perpendicular component remains fluctuating. In the weak XY-case, complete long-range order is gradually achieved towards high fields and $T = 0$ via an increasing uniform component parallel to the field axis. The Bragg intensities measured in phase II at $B = 3.5$ T, $T = 4.80$ K can be reasonably fitted by the collinear fan structure, where only the projection of the spin onto the x-axis is ordered as shown in the upper part of figure 4 (I(calc) in table 1). However, the calculated intensity of $(7/3, 7/3, 1)$ for this structure is too small compared to observation. This indicates the contribution of a spin component perpendicular to $(1, 1, 0)$. Including a partly ordered y- or z-component does not improve the fit significantly, the R-value remaining unchanged. Considering that the phase transitions in this doped compound are rather broad, and the data being taken only $\approx$0.15 K above the II–IV phase boundary, it is probable that the observation of additional intensity at $(7/3, 7/3, 1)$ results from regions of the sample already in phase IV. A two-phase refinement converges to a mixture of $\approx$30% of phase IV and $\approx$70% of phase II (I'(calc) in table 1). As the broadening of T_N at zero field can be described by a Gaussian distribution with $(\mathrm{HWHM})_{T_N} = 0.086$ K, a 30% contribution of phase IV should occur about 0.1 K above T_{N2}. We conclude that the intermediate phase II does indeed exhibit the predicted collinear order.

The observed decrease of all measured magnetic Bragg intensities between the distorted helix and umbrella phases extends over more than 1 T, which is unusually broad for an expected first-order transition. However, the random distribution of Fe^{2+} ions in this doped system has to be taken into consideration, which can drastically broaden the width of the transition due to local variations of anisotropies. Moreover, de Groot and de Jongh [18] argue that soliton excitations in quasi-1d antiferromagnets with XY-anisotropy always lead to a significantly broadened spin-flop transition at finite temperature. On the other hand, an intermediate phase with two second-order phase boundaries—as calculated by Plumer *et al* for a certain configuration of fourth-order anisotropies—cannot be excluded.

The helical zero-field structure is degenerate with respect to a discrete symmetry

operation which reverses the helicity on a given triangle. The theoretically proposed new chiral XY universality class for the $B = 0$ transition exhibits critical exponents considerably different from those of the non-chiral classes [2]. The calculated exponent of the order parameter has the value $\beta = 0.253(10)$ in the chiral XY-class, while it is 0.346(1) in the non-chiral XY-class. Neutron scattering experiments at the tetracritical point of $CsMnBr_3$ have confirmed the chiral XY-value (0.22(2) [19], 0.25(1) [20], 0.24(2) [6]), but no other system has been tested so far. Our value of 0.23(1) is again in excellent agreement with the theoretical value of the chiral XY universality class.

In $CsNi_{0.98}Fe_{0.02}Cl_3$ as in $CsMnBr_3$, $RbMnBr_3$ and $CsVX_3$ (X = Cl, Br, I), the fan phase opens at low magnetic fields between the paramagnetic phase and the distorted helix phase. According to Kawamura *et al* [21] both phase boundaries I–II (paramagnet–fan) and II–III (fan–distorted helix) should follow $H^2 \propto |t|^{\phi}$ with $\phi \approx 1.04$. This behaviour has been observed in $CsMnBr_3$ ($\phi_{I-II} = 1.21(7)$, $\phi_{II-III} = 0.75(5)$ [6], $\phi_{I-II} = 1.02(5)$, $\phi_{II-III} = 1.07(5)$ [22]), $CsVBr_3$ ($\phi_{I-II} = 0.78(6)$, $\phi_{II-III} = 0.79(6)$ [23]) and $RbMnBr_3$ ($\phi_{I-II} = 1.07(25)$, $\phi_{II-III} = 1.00(35)$ [24]). The results for $CsNi_{0.98}Fe_{0.02}Cl_3$ ($\phi_{I-II} = 1.12(9)$, $\phi_{II-III} = 1.01(20)$) fit nicely into this series.

5. Conclusion

From the excellent agreement of the observed magnetic phase diagram with the theoretical predictions we conclude that $CsNi_{0.98}Fe_{0.02}Cl_3$ represents the weak-anisotropy case of a STAL-AF, while $CsMnBr_3$ and $RbMnBr_3$ are examples with strong XY-anisotropy. The $CsVX_3$ compounds are expected to belong to the weak-anisotropy case [13, 14], but this prediction could not be confirmed so far. Hence, in $CsNi_{0.98}Fe_{0.02}Cl_3$, the umbrella phase has been observed for the first time. Our values of β and ϕ confirm once more that the tetracritical $B = 0$ point of a STAL-AF with XY-anisotropy belongs to the new chiral XY universality class, and in addition that doping of $CsNiCl_3$ with Fe^{2+} is an effective means to induce and manipulate XY-anisotropy in this system.

Acknowledgment

Financial support from the Japan Society for the Promotion of Science was essential for this work.

References

[1] Plumer M L, Caillé A and Hood K 1989 *Phys. Rev.* B **39** 4489
[2] Kawamura H 1992 *J. Phys. Soc. Japan* **61** 1299; 1985 *J. Phys. Soc. Japan* **54** 3220
[3] Asano T, Ajiro Y, Mekata M, Katori H and Goto T 1994 *Physica* B **201** 75
[4] Ajiro Y, Asano T, Kadowaki H, Kato T, Kawano S, Katori H and Goto T 1995 *Physica* B **213** 209
[5] Kato T, Ishii T, Ajiro Y, Asano T and Kawano S 1993 *J. Phys. Soc. Japan* **62** 3384
[6] Gaulin B D, Mason T E and Collins M F 1989 *Phys. Rev. Lett.* **62** 1380
[7] Kadowaki H, Ubukoshi K and Hirakawa K 1987 *J. Phys. Soc. Japan* **56** 751
[8] Kadowaki H, Inami T, Ajiro Y, Nakajima K and Endoh Y 1991 *J. Phys. Soc. Japan* **60** 1708
[9] Furtuna G, Enderle M and Steiner M 1994 *J. Phys.: Condens. Matter* **6** L385
[10] Trudeau Y, Plumer M L, Poirier M and Takeuchi J 1995 *Phys. Rev.* B **52** 378
[11] Steiner M, Kakurai K, Knop W, Dorner B, Pynn R, Happek U, Day P and McLeen G 1981 *Solid State Commun.* **38** 1179
[12] *International Tables for X-ray Crystallography* 1974 vol 4 (Birmingham: Kynoch)
[13] Rastelli E and Tassi A 1994 *Phys. Rev.* B **50** 16 475
[14] Abarzhi S I and Chubukov A V 1990 *J. Phys.: Condens. Matter* **2** 9221

[15] Kakurai K, Steiner M, Pynn R and Kjems J K 1991 *J. Phys.: Condens. Matter* **3** 715
[16] Yelon W B and Cox D E 1973 *Phys. Rev.* B **7** 2024
[17] Zhu X and Walker M B 1987 *Phys. Rev.* B **36** 3830
[18] de Groot H J M and de Jongh L J 1986 *Physica* B **141** 1
[19] Mason T E, Gaulin B D and Collins M F 1987 *J. Phys. C: Solid State Phys.* **20** L945
[20] Ajiro Y, Nakashima T, Unno Y, Kadowaki H, Mekata M and Achiwa N 1988 *J. Phys. Soc. Japan* **57** 2648
[21] Kawamura H, Caillé A and Plumer M L 1990 *Phys. Rev.* B **41** 4416
[22] Goto T, Inami T and Ajiro Y 1990 *J. Phys. Soc. Japan* **59** 2328
[23] Tanaka H, Nakano H and Matsuo S 1994 *J. Phys. Soc. Japan* **63** 3169
[24] Heller L, Collins M F, Yang Y S and Collier B 1994 *Phys. Rev.* B **49** 1113